Geophysical Research Letters

RESEARCH LETTER
10.1029/2019GL084215

Sensitivity of Tidewater Glaciers to Submarine Melting Governed by Plume Locations

Tom R. Cowton[1], Joe A. Todd[1], and Douglas I. Benn[1]

[1]School of Geography and Sustainable Development, University of St Andrews, St Andrews, UK

Key Points:
- We use a 3-D numerical model to examine the response of an idealized tidewater glacier to spatial variations in submarine melt rate
- The glacier is most sensitive to melting near the lateral margins, which triggers increased calving across the width of the terminus
- Terminus retreat may thus be paced by the difference between ice velocity and submarine melting across slow flowing marginal zones

Supporting Information:
- Supporting Information S1

Correspondence to:
T. R. Cowton,
tom.cowton@st-andrews.ac.uk

Citation:
Cowton, T. R., Todd, J. A., & Benn, D. I. (2019). Sensitivity of tidewater glaciers to submarine melting governed by plume locations. *Geophysical Research Letters*, *46*. https://doi.org/10.1029/2019GL084215

Received 21 JUN 2019
Accepted 9 SEP 2019
Accepted article online 16 SEP 2019

Abstract The response of tidewater glaciers to ocean warming remains a key uncertainty in sea level rise predictions. Here we use a 3-D numerical model to examine the response of an idealized tidewater glacier to spatial variations in submarine melt rate. While melting toward the center of the terminus causes only a localized increase in mass loss, melting near the lateral margins triggers increased calving across the width of the glacier, causing the terminus to retreat at several times the width-averaged melt rate. This occurs because melting near the margins has a greater disruptive impact on the compressive stress arch that transfers resistance from the side walls to the body of the glacier. We suggest that the rate of terminus advance or retreat may thus be governed by the difference between ice velocity and submarine melting in the slow-flowing zones away from the glacier center.

Plain Language Summary The rapid retreat of tidewater glaciers (i.e., glaciers that drain directly into the ocean) has become an increasing source of concern in recent years. Increased melting of the submerged parts of these glaciers by warming ocean waters is thought to be an important driver of this retreat, but exactly how glaciers respond to this submarine melting remains unclear. Using a numerical model, we find that tidewater glaciers may be most sensitive to melting close to the valleysides, which reduces structural support for the central section of the glacier and so triggers an increase in iceberg calving. By better constraining the relationships between submarine melting, calving, and glacier retreat, our findings allow improved prediction of the ice loss expected from tidewater glaciers as the climate continues to warm.

1. Introduction

The rapid retreat of many tidewater glaciers in recent decades has been attributed to an increase in submarine melting in response to warming oceanic and atmospheric conditions (Straneo & Heimbach, 2013), yet the associated mechanisms remain poorly understood. The process appears intuitive if submarine melt rates are of a comparable magnitude to glacier velocity, such that submarine melting represents a substantial component of the mass budget at the terminus (e.g., Bartholomaus et al., 2013; Luckman et al., 2015; Slater et al., 2017). At many larger- and faster-flowing glaciers, however, estimated submarine melt rates fall far below ice velocity, with most ice lost to the sea through calving (e.g., James et al., 2014; Rignot et al., 2016; Sutherland & Straneo, 2012). At these glaciers, it is less clear if and how submarine melting can act as the primary driver of terminus retreat.

One possibility is that an increase in submarine melting leads in turn to an increase in calving. This "calving multiplier" was first hypothesized by O'Leary and Christoffersen (2013), who proposed that melt undercutting of a glacier terminus could increase the size of calving events by displacing bending stresses up glacier. Subsequent studies using more realistic, time-evolving models have however proven equivocal as to the significance of this mechanism (Benn et al., 2017; Cook et al., 2014; Krug et al., 2015; Ma & Bassis, 2019; Todd & Christoffersen, 2014) and whether submarine melting can drive a significant calving multiplier effect thus remains unclear.

A commonality in these studies is that they have been based on the use of 2-D models that represent a longitudinal slice through the glacier terminus. Because of this, the possible significance of lateral variations in ice velocity and submarine melt rates have received less attention. Even in a simplistic scenario in which submarine melt rates are spatially uniform, the balance between ice advection and melting will vary across the calving front due to spatial variations in ice velocity (Wagner et al., 2019). In reality, it is likely that submarine melt rates are also highly spatially heterogenous due to the complexities of near-terminus circulation

and water properties such as temperature and salinity (Slater et al., 2018). In particular, where the runoff of freshwater from channels at the glacier bed drives buoyant plumes adjacent to the calving front (e.g., Chauché et al., 2014; Xu et al., 2013), submarine melting may be an order of magnitude more rapid than elsewhere on the calving front (Slater et al., 2015).

While these plumes have attracted considerable interest in recent years, their significance for glacier stability remains unclear. Because individual plumes cover only a small part of the calving front, the amount of ice lost directly to plume melting is often likely to be relatively small, despite the locally high melt rates (Truffer & Motyka, 2016). As such, plume melting seems only likely to be able to drive glacier retreat if it has a destabilizing influence on a wider part of the terminus, causing an accompanying increase in calving. For this to happen, plume melting must modify the near-terminus stress fields that dictate the location and magnitude of calving events (Benn et al., 2007).

A feature of these stress fields that has attracted attention at floating ice shelves, but comparatively little with respect to tidewater glaciers, is the existence of a "compressive arch" upstream of the calving front (Doake et al., 1998; Kulessa et al., 2014). This arch marks the downstream transition to a zone where both horizontal principal stresses or strains are extensional (upstream of this location, the second principal stress is compressive due to the transfer of resistance from the glacier margins), and ice is thus liable to fracture and calve. In this way, the compressive arch determines the stable position of the terminus (Doake et al., 1998); as ice is advected beyond this point, extensional stresses increase until calving occurs. If submarine melting is sufficient to cause even localized disruptions to this arch, this may have the effect of reducing lateral support to the body of the glacier and forcing these stress patterns to migrate upglacier, decreasing the stability of near-terminus ice. This would effectively shift the stable location of the terminus upglacier, likely resulting in an increase in the calving rate and eventual retreat of the calving front back to a new stable location.

Modification of the near-terminus stress fields thus provides a possible mechanism through which localized areas of mass imbalance on the calving front (due to higher melt rates and/or slower ice velocities) may have a glacier-wide impact on frontal mass loss and thus glacier retreat, causing a calving multiplier effect overlooked by previous 2-D modeling studies. This possibility was highlighted by Todd et al. (2018, 2019), who, using a 3-D ice flow model of Store Glacier in west Greenland, found that the addition of plume melting zones significantly increased the seasonal retreat of the terminus, a response which they attributed to the breaking of lateral stress bridges. In this paper, we use a similar model setup, applied to an idealized tidewater glacier, to focus in detail on this effect. By examining the response of the modeled glacier to laterally variable submarine melt rates, we are able to demonstrate that this mechanism can be an important control on tidewater glacier stability, capable of driving glacier retreat at several times the spatially averaged submarine melt rate.

2. Methods

Modeling experiments are undertaken using Elmer/Ice, a finite-element ice flow model that solves the full Stokes equations (Gagliardini et al., 2013). We use an idealized, 3-D geometry for a simple tidewater glacier with parallel vertical sides, 4,000 m apart, and a flat bed that slopes linearly seaward except for a shallow bump at the terminus (Figure S1 in the supporting information). The model uses an unstructured grid, with nine vertical layers and linear prism elements with a minimum size (at the terminus) of ~50 m. We use a Glen-type rheology ($n = 3$). Basal and lateral drag are defined by a Coulomb-style friction law (Gagliardini et al., 2007); in the main experiments, we use sliding coefficients of 1×10^{6} and 1×10^{-3}, respectively, with alternative values tested in the sensitivity analysis (Table S1). Both the surface and basal boundary are allowed to evolve freely through time, including ungrounding (and an associated loss of basal friction) as the glacier reaches flotation. At the base and the submarine portion of the calving front, we apply a hydrostatic external pressure from the fjord. Inflow into the domain, ~15 km from the terminus, is 800 m/year. At the calving front, ice is ~360 m thick and flowing at a mean velocity of ~570 m/year (Figure S11).

Calving is implemented in the model using a 3-D crevasse depth type calving law (Benn et al., 2007; Nye, 1957; Todd et al., 2018). Full details of the scheme are provided by Todd et al. (2018); to outline briefly, zones of crevasse formation are approximated based on the effective principal stress (σ_p)

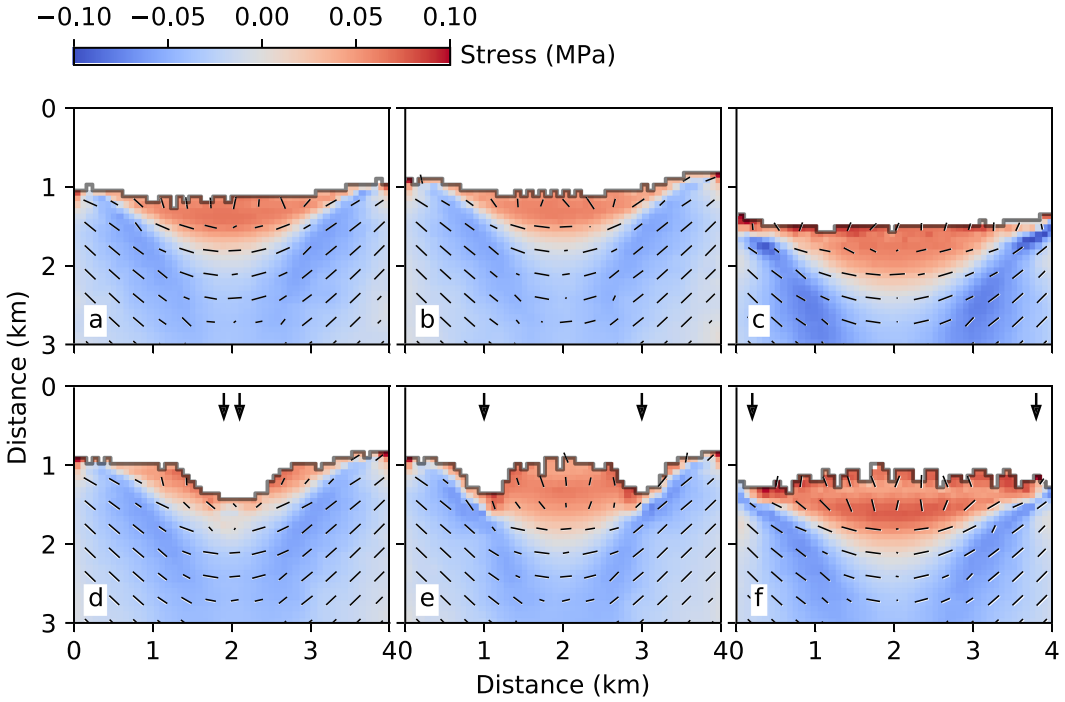

Figure 1. Plan views of the terminus showing the magnitude and orientation of the second horizontal principal stress. Blue and red shadings denote areas of compressional and extensional stresses, respectively, with the downstream limit of the compressive arch lying at the boundary between these two zones. (a) Initial conditions and (b–f) end of season conditions for the (b) no melt, (c) distributed melt, (d) central plumes, (e) intermediate plumes, and (f) marginal plumes experiments (with melt rate = 2,000 m/year). Black arrows show plume locations. Model outputs have been interpolated onto a regular 75-m grid for plotting.

$$\sigma_{\mathrm{p,surface}} = \sigma_1 \tag{1}$$

$$\sigma_{\mathrm{p,basal}} = \sigma_1 + P_w, \tag{2}$$

where σ_1 is the largest principal stress and P_w is water pressure (equal to the hydrostatic pressure of sea water). Crevasse fields are predicted to form where σ_p is positive. Calving occurs when the surface crevasse field either intersects the waterline or joins with the predicted basal crevasse field such that a portion of the calving front becomes isolated and can be detached to leave a vertical calving front (Todd et al., 2018). We emphasize that the calving law is designed to reproduce calving patterns at the broad scale and not accurately capture individual calving events. Because the calving law is based on an approximation of the instantaneous crevasse field, it is also unable to represent the calving of large icebergs through the gradual propagation of rifts across the glacier.

Submarine melting is implemented by adjusting the displacement of the terminus mesh nodes to reflect the balance between advection and melting (see Todd et al., 2018, equation 15). The model is spun up by allowing the glacier to advance without submarine melting until it reaches the desired extent. For the main experiments, this extent is defined as when the terminus reaches 95% of flotation (Figure 1a), although we also consider an alternative scenario with a small floating tongue (Table S1). We then run experiments with plume melting switched on for 120 days, representing the summer melt season. In the main experiments plume melting is applied across 200 m wide zones, reflecting observations indicating that relatively wide "truncated line plumes" are likely more realistic than narrow point source plumes (Fried et al., 2015; Jackson et al., 2017), while 100 and 300 m wide variants are tested in the sensitivity analysis (Table S1). Melt rates are laterally and vertically uniform within these plume zones, and we do not apply submarine melting outside of the plume zones or on the base of floating ice. For comparison, we do however also include experiments in which the same melt rates are applied as "distributed melting," uniformly across the entire calving front.

For each suite of experiments, we explore the response of the glacier to variations in plume melt rate and location. We apply plume melt rates of 0, 500, 1,000, 1,500, and 2,000 m/year to the calving front, which are kept constant for the duration of the experiment. We use three plume locations, termed *marginal*, *intermediate*, and *central*, corresponding to plume-center distances of 200, 1,000, and 2,000 m, respectively, from the ice margin (arrows in Figures 1d–1f). In the main experiments we include two equally sized plumes, located at equal distances from opposing glacier margins (for the central plume location, we simply make the plume twice as wide), with a single plume scenario considered in the sensitivity analysis (Table S1).

3. Results

In the absence of submarine melting, the terminus slowly advances at an average rate of ~320 m/year (Figures 1a and 1b). The addition of plumes to the center of the calving front results in the formation of a substantial notch, but has little impact on the shape and position of the wider calving front (Figure 1d). The incised notch is contained wholly within the extensional zone of the stress field, with no impact on the form or position of the compressive arch. Similarly, the impact of plumes positioned in the intermediate locations (Figure 1e) is largely restricted to the formation of two large notches in the calving front. These are initially contained within the extensional zone, but melt through this over the course of the melt season, slightly displacing the compressive arch upstream.

Placing the plumes close to the glacier margins has a markedly different impact (Figure 1f). Because the extensional zone here is narrow, plume melting rapidly cuts into the compressive arch, removing fjord wall support from some of the central part of the glacier. The arch is thus displaced upglacier, increasing the area and magnitude of extensional stresses, and hence potential calving, across the width of the terminus. Likewise, if melting is applied universally across the calving front, there is rapid retreat across the full width of the glacier (Figure 1c). The retreat of the compressive arch is similar to the marginal plumes scenario, but ice from across the width of the glacier is more rapidly removed, resulting in a flatter terminus shape and a greater overall retreat.

These changes can be quantified by looking at the relationship between width-averaged submarine melt rate, m_{av}, and the width-averaged rate of change of the position of the terminus (P_T) and compressive arch (P_A; Figure 2). To examine this, we define the calving multiplier value k_i as

$$\frac{\mathrm{d}P_i}{\mathrm{d}t} = \frac{\mathrm{d}P_{0,i}}{\mathrm{d}t} - k_i m_{\mathrm{av}} \tag{3}$$

where the subscript $i = T$ or A, depending on whether the terminus T or compressive arch A is being considered. $P_{0,\mathrm{i}}$ is the equivalent position in the absence of submarine melting. For both the central and intermediate plume positions we find $k_T = 0.7$ (Figure 2a and Table S1); being <1, this indicates that increased melting in the extensional zone has caused a corresponding decrease in calving, as ice that would otherwise calve is removed. Conversely, with the plumes in the marginal location there is a significant calving multiplier effect, with $k_T = 2.6$ (Figure 2a, and Table S1). This occurs because plume melting forces the retreat of the compressive arch (Figure 1f), increasing calving rates across the width of the terminus and so amplifying the impact of the melting on terminus position.

These trends become clearer if the retreat of the compressive arch is considered (Figure 2c). Plumes in the central location have negligible impact on the compressive arch, with melt rates insufficient to cut through the extensional zone over the course of the melt season. There is a small retreat of the compressive arch in the intermediate plume location scenario ($k_A = 1.8$), but a far greater impact is felt when plumes are in the marginal location, with $k_A = 6.6$ (Figure 2c and Table S1). Although the highest retreat rates are found in the distributed melt scenario, the much higher width-averaged melt rates greatly reduce the multipliers, resulting in values for k_T and k_A of only 1.2 and 1.4, respectively (Figures 2a, 2c, and Table S1).

Further insight into these results can be gained by looking at the relationship between retreat rate and the local melt rate m_{loc} (i.e., the melt rates applied within the melt zones) rather than the width-averaged melting. For a given local melt rate, terminus retreat is more than twice as rapid in the distributed melt scenario compared to the marginal plumes scenario (Figure 2b). However, when the retreat of the compressive arch is considered, the difference between these two scenarios is much reduced (Figure 2d), with only a slightly

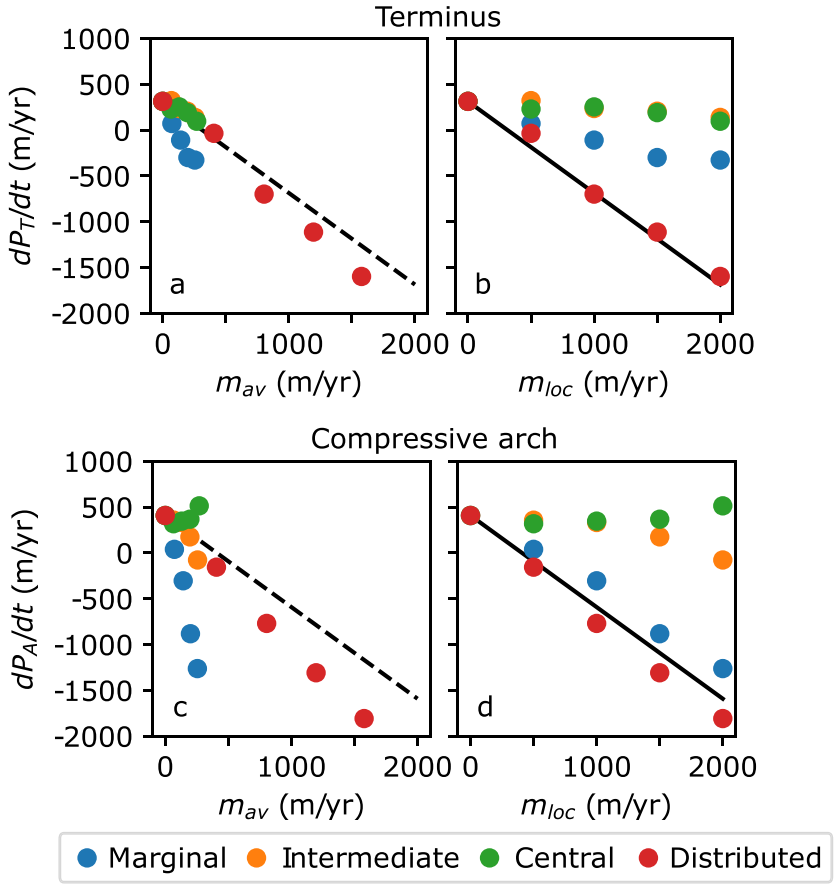

Figure 2. Relationship between (a) width-averaged melt rate, m_{av}, or (b) local melt rate (within melt zones), m_{loc}, and width-averaged rate of change in the terminus position, dP_T/dt (positive = advance). (c, d) As in (a, b) but for rate of change of compressive arch position, dP_A/dt. Dashed black line in (a) and (c) shows the relationship described by equation (3) with $k_i = 1$, while the solid black line in (b) and (d) shows the relationship described by equation (4).

more rapid retreat in the distributed melting scenario. The impact on the near-terminus stress fields is thus very similar regardless of whether melting is applied to the full calving front or just to two key zones toward the glacier margins, where it can most effectively impact the compressive stress arch. The difference in the rate of calving front retreat (Figure 2b) then depends on the rate at which the destabilized central part of the calving front (Figure 1f) loses ice in the model.

4. Interpretation and Discussion

4.1. Controls on Retreat Rate

Our results highlight the importance of the near-terminus stress field in modulating the impact of submarine melting on tidewater glaciers. In particular, the impact of the applied submarine melting on the modeled terminus depends on whether or not it disturbs the compressive arch. If melting removes ice from only the extensional zone, which contributes little to glacier stability, the effect is largely local (Figures 1d and 1e). If, however, the melting disrupts the compressive arch, the changing stress field can decrease stability and thus increase calving across a much wider part of the glacier (Figure 1f). A localized plume may therefore be able to force the retreat of a glacier even if it only directly affects a small area of the terminus, so long as this area is a sensitive location with respect to the near-terminus stress field: we find that a given melt rate, applied in two 200 m wide zones toward the glacier margins, drives almost as rapid a retreat of the compressive arch as when the same melt rate is applied across the full 4,000 m wide calving front (Figures 1c, 1d, and 1f).

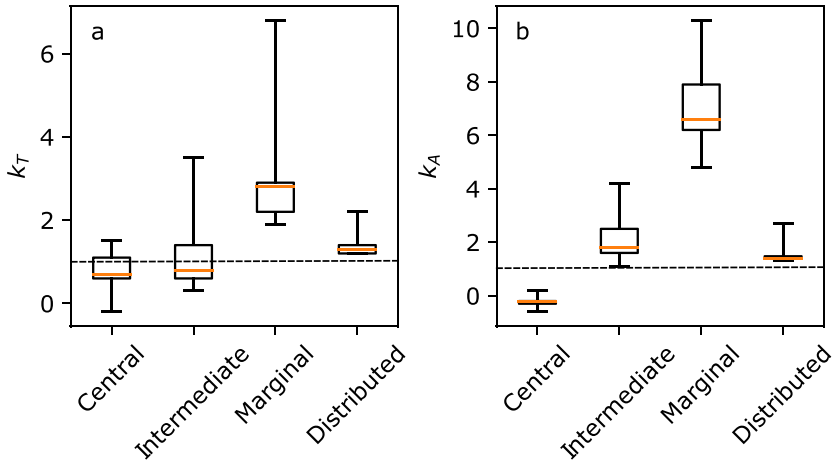

Figure 3. Box plots showing values of (a) k_T and (b) k_A from the sensitivity experiments (Table S1). Plots show the median value (orange line), interquartile range (box) and full range (whiskers). Values lying above the dashed lines at k_T and $k_A = 1$ indicate an enhancement of calving and compressive arch retreat. For each melt location, $n = 9$, except for distributed melt ($n = 6$). Values are plotted individually in Figure S10.

It is evident from the results that melting toward the glacier margins has a much greater impact on the compressive arch, and hence the wider terminus stability, than melting toward the center of the glacier. The reasons for this are threefold. First, at the margins the compressive arch is not protected by a buffer of extensional ice, as it is toward the glacier center. Second, toward the margins ice is slower flowing, and so a given melt rate results in a larger retreat than if applied to the fast-flowing ice toward the center. Third, a disruption to the arch toward the margins (Figure 1f) forces an upglacier displacement of this structure across a wider proportion of the glacier relative to melting closer to the glacier center (Figure 1e).

If the compressive arch determines the stable position of the glacier terminus, then our findings suggest that the rate of advance or retreat of a tidewater glacier may be approximated simply as the difference between the local ice velocity, u_{loc}, and submarine melt rate, m_{loc}, across those zones where the compressive arch is most vulnerable:

$$\frac{\mathrm{d}P_{T,A}}{\mathrm{d}t} = u_{\mathrm{loc}} - m_{\mathrm{loc}} \tag{4}$$

In keeping with equation (4), in the absence of melt, the modeled glacier advances at the speed of the marginal ice rather than the faster-flowing ice in the glacier center (Figures 2b and S11). As increasing melting is applied at the margins, we find that equation (4) provides a good approximation of the rate of retreat of the compressive arch in both the marginal plumes and distributed melt scenarios (Figure 2d), and of the terminus in the distributed melting scenario (Figure 2b). Equation (4) does, however, overestimate terminus retreat relative to the model for the marginal plumes scenario (Figure 2b). This is because while modeled calving rates increase across the newly enlarged extensional zone, they do not keep pace with the melting at the margins, resulting in the formation of a central bulge in the terminus (Figure 1f). It seems likely, however, that should the compressive arch remain in this location for sufficient time, the elevated calving rates would cause the retreat of the central section of the terminus until a more stable, concave geometry is reached (e.g., Figures 1a and 1b).

Changes in the stable position of the terminus are thus paced by the difference between melt rate and ice velocity toward the glacier margins. An important implication of this is that the width-averaged terminus retreat due to submarine melting is likely to occur at a rate more rapid than the width-averaged velocity minus the width-averaged melt rate. Even when melting is evenly distributed across the calving front, terminus retreat occurs primarily as a function of the difference between melt rate and velocity toward the margins (Figures 1c and 2b). This paces retreat across the rest of the front by changing the stress field and increasing calving rates, resulting in a small calving multiplier effect (Figures 1c, 2d, and

Table S1). If melting is concentrated at the margins, the calving multiplier effect is much more sensitive, such that the change in retreat rate may be several times greater than the change in width-averaged melt rate (Figure 2a and Table S1). This is important, as it means that submarine melting may be a significant control on terminus position even at faster-flowing glaciers where average melt rates remain below ice velocities.

4.2. Sensitivities

We test the sensitivity of our findings to the number and extent of plumes, the relative importance of basal and lateral drag, and the presence or absence of a floating ice tongue (Table S1 and Figures S2–S10). The heightened sensitivity to melt in the marginal plume locations is a robust feature of the results, though there is a considerable spread in the range of values of k_T and k_A (Figure 3). Reducing the plume width to 100 m results in some of the highest multiplier values ($k_T = 4.8$ and $k_A = 10.3$ for the marginal plumes scenario); although wider plumes result in greater retreat in absolute terms, the impact per unit melt decreases as the area affected by melting increases (Table S1 and Figure S10). Also of importance is the relative magnitude of basal and lateral drag: if lateral drag contributes more to the glacier force balance, the stress arch becomes more strongly defined (e.g., Figure S6 compared to Figure S5) and the glacier becomes increasingly sensitive to melting by the marginal plumes. We find that for a $\pm$ 80% change in the basal/lateral friction law coefficients (resulting in a change in mean terminus velocity of up ~70%; Figure S11), k_T varies by up to ~25% (Table S1). The compressive arch is therefore likely to be of greatest significance at glaciers where lateral drag is important, in keeping with the original focus on compressive arches at floating ice shelves (Doake et al., 1998; Kulessa et al., 2014), at which all resistance to flow is provided by lateral rather than basal drag. Indeed, the highest value of k_T that we obtain (6.8 for the marginal plumes scenario) is for a scenario in which the terminus is allowed to form a floating tongue, which rapidly disintegrates when subject to melting. In contrast to previous work with vertical 2-D models, which found floating ice to be relatively insensitive to melt undercutting (Benn et al., 2017), this therefore highlights that the response to localized submarine melting may be even stronger where a floating tongue exists.

4.3. Applicability to Real Glaciers

Our findings provide a plausible explanation for the sensitivity of glaciers to fjord water temperature even when average submarine melt rates likely fall below average ice velocities (e.g., Khazendar et al., 2019; Luckman et al., 2015). Partitioning the mass budget at tidewater glaciers remains highly challenging, however (Wagner et al., 2019), limiting our ability to test these theoretical predictions. One interesting strand of evidence comes from detailed time lapse imagery of Rink Isbrae, west Greenland (Medrzycka et al., 2016), which showed that the calving front could be divided into two zones: slower-flowing, melt-dominated margins, and a faster-flowing central trunk in which major calving events are dictated by the wider stress fields—a configuration in good agreement with the mechanisms presented here. Similarly, at Saqqarliup Glacier, also in west Greenland, Wagner et al. (2019) suggested that mass loss from the central trunk of the glacier may be influenced by two proximal melt-dominated zones associated with plume activity. Indeed, observations commonly indicate the presence of one or more plumes in locations significantly offset from the glacier center (e.g., Chauché et al., 2014; How et al., 2017; Slater et al., 2018). High resolution 3-D modeling of Greenland's outlet glaciers (e.g., Todd et al., 2018, 2019), supported by detailed observations of ice flow and hydrology, may help to determine the sensitivity of these systems to the spatial distribution of submarine melting.

There are inevitably some complications when applying this theory to real-world scenarios compared to the idealized glacier modeling. In particular, the stress field, including the position and form of the compressive arch, will be more complex for actual glacier geometries. With uneven bed topography, a less clear transition between the glacier bed and walls, and zones of weakened ice along shear margins, the key areas for submarine melting may not simply lie close to the visible fjord walls as in the idealized glacier experiments. Similarly, a stable compressive arch position may be associated with a particular topographic pinning point (Doake et al., 1998, Kulessa et al., 2014); if the glacier is displaced from this point, then this may result in a period of dynamic retreat, independent of melt rates, until a new stable location is reached (e.g., Catania et al., 2018). Thus, in some scenarios, there may be a critical compressive arch position beyond which a phase of runaway retreat is expected, while in others the compressive arch may be able to transition relatively smoothly up and down fjord at a rate determined by ice velocity and submarine melt rates.

5. Conclusions

Our findings indicate that the response of a glacier to submarine melting is highly dependent on the spatial distribution of melting. If melting is confined to the zone of extensional stresses toward the center of the glacier, the impact is largely local and limited in magnitude. If, however, melting is able to disrupt the compressive arch that surrounds this zone, it can increase calving across the full width of the glacier, driving terminus retreat. This means that glaciers may be much more sensitive to melt near the margins than in the center of the calving front. Our experiments indicate that for a simplified bed topography, the rate of advance or retreat of the stable terminus position is paced by the difference between melt rate and ice velocity across a zone a few hundred meters in width adjacent to the glacier margins, providing a simple method for estimating the response of a glacier to a change in submarine melting. This remains the case whether melting is applied in concentrated plume zones or uniformly across the entire terminus, though can be exceeded if melting triggers the breakup of a floating tongue. The retreat rate is thus often greater than the difference between the width-averaged melt rate and ice velocity, by as much as a factor of 5 or more in the plume melting scenarios. These findings therefore suggest that even large and fast flowing glaciers may be sensitive to changes in submarine melting, particularly when the relatively slow-flowing marginal areas are subject to intense plume melting. Greater attention should therefore be given to spatial variation in melt rate and ice velocity across the calving front, and the ability of local flux imbalances to affect the stress fields that dictate terminus stability.

Acknowledgments
The code constituting the 3-D calving model has been made freely available via integration with the Elmer/Ice source code, available at this site (https://github.com/ElmerCSC/elmerfem/tree/elmerice). The model configuration files required to reproduce the experiments shown in the paper are provided in the supporting information. This work was funded by NERC Award NE/P011365/1 (CALISMO: Calving laws for Ice Sheet Models) to PI Benn. We would like to thank two anonymous referees for their insightful feedback on the manuscript.

References

Bartholomaus, T. C., Larsen, C. F., & O'Neel, S. (2013). Does calving matter? Evidence for significant submarine melt. *Earth and Planetary Science Letters*, *380*, 21–30. https://doi.org/10.1016/j.epsl.2013.08.014

Benn, D. I., Åström, J., Zwinger, T., Todd, J., Nick, F. M., Cook, S., et al. (2017). Melt-under-cutting and buoyancy-driven calving from tidewater glaciers: New insights from discrete element and continuum model simulations. *Journal of Glaciology*, *63*(240), 691–702. https://doi.org/10.1017/jog.2017.41

Benn, D. I., Warren, C. R., & Mottram, R. H. (2007). Calving processes and the dynamics of calving glaciers. *Earth-Science Reviews*, *82*(3-4), 143–179. https://doi.org/10.1016/j.earscirev.2007.02.002

Catania, G., Stearns, L., Sutherland, D., Fried, M., Bartholomaus, T., Morlighem, M., et al. (2018). Geometric controls on tidewater glacier retreat in central western Greenland. *Journal of Geophysical Research: Earth Surface*, *123*, 2024–2038. https://doi.org/10.1029/2017JF004499

Chauché, N., Hubbard, A., Gascard, J. C., Box, J. E., Bates, R., Koppes, M., et al. (2014). Ice-ocean interaction and calving front morphology at two west Greenland tidewater outlet glaciers. *The Cryosphere*, *8*(4), 1457–1468. https://doi.org/10.5194/tc-8-1457-2014

Cook, S., Rutt, I. C., Murray, T., Luckman, A., Zwinger, T., Selmes, N., et al. (2014). Modelling environmental influences on calving at Helheim Glacier in eastern Greenland. *The Cryosphere*, *8*(3), 827–841. https://doi.org/10.5194/tc-8-827-2014

Doake, C., Corr, H., Rott, H., Skvarca, P., & Young, N. (1998). Breakup and conditions for stability of the northern Larsen Ice Shelf, Antarctica. *Nature*, *391*(6669), 778. https://doi.org/10.1038/35832

Fried, M. J., Catania, G. A., Bartholomaus, T. C., Duncan, D., Davis, M., Stearns, L. A., et al. (2015). Distributed subglacial discharge drives significant submarine melt at a Greenland tidewater glacier. *Geophysical Research Letters*, *42*, 1944–8007. https://doi.org/10.1002/2015GL065806

Gagliardini, O., Cohen, D., Råback, P., & Zwinger, T. (2007). Finite-element modeling of subglacial cavities and related friction law. *Journal of Geophysical Research*, *112*, F02027. https://doi.org/10.1029/2006JF000576

Gagliardini, O., Zwinger, T., Gillet-Chaulet, F., Durand, G., Favier, L., de Fleurian, B., et al. (2013). Capabilities and performance of Elmer/Ice, a new-generation ice sheet model. *Geoscientific Model Development*, *6*(4), 1299–1318. https://doi.org/10.5194/gmd-6-1299-2013

How, P., Benn, D. I., Hulton, N. R., Hubbard, B., Luckman, A., Sevestre, H., et al. (2017). Rapidly changing subglacial hydrological pathways at a tidewater glacier revealed through simultaneous observations of water pressure, supraglacial lakes, meltwater plumes and surface velocities. *The Cryosphere*, *11*, 2691–2710. https://doi.org/10.5194/tc-11-2691-2017

Jackson, R. H., Shroyer, E. L., Nash, J. D., Sutherland, D. A., Carroll, D., Fried, M. J., et al. (2017). Near-glacier surveying of a subglacial discharge plume: implications for plume parameterizations. *Geophysical Research Letters*, *43*, 6886–6894. https://doi.org/10.1002/2017GL073602

James, T. D., Murray, T., Selmes, N., Scharrer, K., & O'Leary, M. (2014). Buoyant flexure and basal crevassing in dynamic mass loss at Helheim Glacier. *Nature Geoscience*, *7*(8), 594–597. https://doi.org/10.1038/ngeo2204

Khazendar, A., Fenty, I. G., Carroll, D., Gardner, A., Lee, C. M., Fukumori, I., et al. (2019). Interruption of two decades of Jakobshavn Isbrae acceleration and thinning as regional ocean cools. *Nature Geoscience*, *12*(4), 277–283. https://doi.org/10.1038/s41561-019-0329-3

Krug, J., Durand, G., Gagliardini, O., & Weiss, J. (2015). Modelling the impact of submarine frontal melting and ice mélange on glacier dynamics. *The Cryosphere*, *9*, 989–1003. https://doi.org/10.5194/tc-9-989-2015

Kulessa, B., Jansen, D., Luckman, A. J., King, E. C., & Sammonds, P. R. (2014). Marine ice regulates the future stability of a large Antarctic ice shelf. *Nature Communications*, *5*, 3707. https://doi.org/10.1038/ncomms4707

Luckman, A., Benn, D. I., Cottier, F., Bevan, S., Nilsen, F., & Inall, M. (2015). Calving rates at tidewater glaciers vary strongly with ocean temperature. *Nature Communications*, *6*. https://doi.org/10.1038/ncomms9566

Ma, Y., & Bassis, J. N. (2019). The effect of submarine melting on calving from marine terminating glaciers. *Journal of Geophysical Research: Earth Surface*, *124*, 334–346. https://doi.org/10.1029/2018JF004820

Medrzycka, D., Benn, D. I., Box, J. E., Copland, L., & Balog, J. (2016). Calving Behavior at Rink Isbræ, West Greenland, from time-lapse photos. *Arctic, Antarctic, and Alpine Research*, *48*(2), 263–277. https://doi.org/10.1657/AAAR0015-059

Nye, J. F. (1957). The distribution of stress and velocity in glaciers and ice-sheets. *Proceedings of the Royal Society of London, Series A. Mathematical and Physical Sciences*, *239*(1216), 113–133. https://doi.org/10.1098/rspa.1957.0026

O'Leary, M., & Christoffersen, P. (2013). Calving on tidewater glaciers amplified by submarine frontal melting. *The Cryosphere*, *7*(1), 119–128. https://doi.org/10.5194/tc-7-119-2013

Rignot, E., Xu, Y., Menemenlis, D., Mouginot, J., Scheuchl, B., Li, X., et al. (2016). Modeling of ocean-induced ice melt rates of five west Greenland glaciers over the past two decades. *Geophysical Research Letters*, *43*, 6374–6382. https://doi.org/10.1002/2016gl068784

Slater, D., Straneo, F., Das, S. B., Richards, C. G., Wagner, T., & Nienow, P. (2018). Localized plumes drive front-wide ocean melting of a Greenlandic tidewater glacier. *Geophysical Research Letters*, *45*, 12,350–12,358. https://doi.org/10.1029/2018GL080763

Slater, D. A., Nienow, P. W., Cowton, T. R., Goldberg, D. N., & Sole, A. J. (2015). Effect of near-terminus subglacial hydrology on tidewater glacier submarine melt rates. *Geophysical Research Letters*, *42*, 2861–2868. https://doi.org/10.1002/2014gl062494

Slater, D. A., Nienow, P. W., Goldberg, D. N., Cowton, T. R., & Sole, A. J. (2017). A model for tidewater glacier undercutting by submarine melting. *Geophysical Research Letters*, *44*, 2360–2368. https://doi.org/10.1002/2016gl072374

Straneo, F., & Heimbach, P. (2013). North Atlantic warming and the retreat of Greenland's outlet glaciers. *Nature*, *504*(7478), 36–43. https://doi.org/10.1038/nature12854

Sutherland, D. A., & Straneo, F. (2012). Estimating ocean heat transports and submarine melt rates in Sermilik Fjord, Greenland, using lowered acoustic Doppler current profiler (LADCP) velocity profiles. *Annals of Glaciology*, *53*(60), 50–58. https://doi.org/10.3189/2012AoG60A050

Todd, J., & Christoffersen, P. (2014). Are seasonal calving dynamics forced by buttressing from ice melange or undercutting by melting? Outcomes from full-Stokes simulations of Store Glacier, West Greenland. *The Cryosphere*, *8*(6), 2353–2365. https://doi.org/10.5194/tc-8-2353-2014

Todd, J., Christoffersen, P., Zwinger, T., Råback, P., & Benn, D. I. (2019). Sensitivity of calving glaciers to ice-ocean interactions under climate change: New insights from a 3D full-Stokes model. *The Cryosphere*, *2019*, 1–21. https://doi.org/10.5194/tc-2019-20

Todd, J., Christoffersen, P., Zwinger, T., Råback, P., Chauché, N., Benn, D., et al. (2018). A full-Stokes 3-D calving model applied to a large Greenlandic glacier. *Journal of Geophysical Research: Earth Surface*, *123*, 410–432. https://doi.org/10.1002/2017JF004349

Truffer, M., & Motyka, R. J. (2016). Where glaciers meet water: Subaqueous melt and its relevance to glaciers in various settings. *Reviews of Geophysics*, *54*, 220–239. https://doi.org/10.1002/2015RG000494

Wagner, T., Straneo, F., Richards, C. G., Slater, D., Stevens, L. A., Das, S., & Singh, H. (2019). Large spatial variations in the flux balance along the front of a Greenland tidewater glacier. *Cryosphere*, *13*(3), 911–925. https://doi.org/10.5194/tc-13-911-2019

Xu, Y., Rignot, E., Fenty, I., Menemenlis, D., & Flexas, M. M. (2013). Subaqueous melting of Store Glacier, west Greenland from three-dimensional, high-resolution numerical modeling and ocean observations. *Geophysical Research Letters*, *40*, 4648–4653. https://doi.org/10.1002/grl.50825